Journal Pre-proof

PPARγ Agonist Attenuates Vocal Fold Fibrosis in Rats via Regulation of Macrophage Activation

Shinji Kaba, Yoshitaka Kawai, Yuki Tanigami, Hiroe Ohnishi, Tomoko Kita, Masayoshi Yoshimatsu, Koichi Omori, Yo Kishimoto

PII: S0002-9440(22)00052-9

DOI: https://doi.org/10.1016/j.ajpath.2022.02.002

Reference: AJPA 3712

To appear in: *The American Journal of Pathology*

Received Date: 19 August 2021

Revised Date: 19 January 2022

Accepted Date: 7 February 2022

Please cite this article as: Kaba S, Kawai Y, Tanigami Y, Ohnishi H, Kita T, Yoshimatsu M, Omori K, Kishimoto Y, PPARγ Agonist Attenuates Vocal Fold Fibrosis in Rats via Regulation of Macrophage Activation, *The American Journal of Pathology* (2022), doi: https://doi.org/10.1016/j.ajpath.2022.02.002.

PPARγ Agonist Attenuates Vocal Fold Fibrosis in Rats via Regulation of Macrophage Activation

Running head: Pioglitazone and vocal fold fibrosis

Authors: Shinji Kaba, Yoshitaka Kawai, Yuki Tanigami, Hiroe Ohnishi, Tomoko Kita, Masayoshi Yoshimatsu, Koichi Omori, and Yo Kishimoto

Affiliations: Department of Otolaryngology-Head and Neck Surgery, Graduate School of Medicine, Kyoto University, Kyoto, Japan

Number of text pages: 16

Number of tables: NA **Number of figures:** 6

Grant numbers and sources of support: Grants-in-Aid for Scientific Research from the Japan Society for the Promotion of Science (17K11381, 20K09730) and GSK Japan Research Grant 2016.

Disclosures: The authors declare no conflicts of interest.

Corresponding author: Yo Kishimoto, MD, Ph.D., Department of Otolaryngology-Head and Neck Surgery, Graduate School of Medicine, Kyoto University, 54 Kawahara-cho, Shogoin, Sakyo-ku, Kyoto 606-8507, Japan.

Phone: +81-75-751-3346

Fax: +81-75-751-7225

Email: y_kishimoto@ent.kuhp.kyoto-u.ac.jp

Abstract

Macrophages aid in wound healing by changing their phenotype and can be a key driver of fibrosis. However, the contribution of macrophage phenotype to fibrosis following vocal fold injury remains unclear. Peroxisome proliferator-activated receptor-γ (PPARγ) is expressed mainly by macrophages during early wound healing and regulates the macrophage phenotype. This study aimed to evaluate the effects of pioglitazone, a PPARγ agonist, on the macrophage phenotype and fibrosis following vocal fold injury in rats. Pioglitazone was injected into the rats' vocal folds on days 1, 3, 5, and 7 after injury, and the vocal fold lamina propria was evaluated on days 4 and 56 after injury. Moreover, THP-1-derived macrophages were treated with pioglitazone, and the expression of pro-inflammatory cytokines under lipopolysaccharide/interferon-γ stimulation was analyzed. The results revealed that pioglitazone reduced the expression of *Ccl2* both *in vivo* and *in vitro*. Furthermore, pioglitazone decreased the density of inducible nitric oxide synthase^{+} CD68^{+} macrophages and inhibited the expression of fibrosis-related factors on day 4 after injury. On day 56 after injury, pioglitazone inhibited fibrosis, tissue contracture, and hyaluronic acid loss in a PPARγ-dependent manner. These results indicate that PPARγ activation could inhibit accumulation of inflammatory macrophages and improve tissue repair. Considered together, these findings imply that inflammatory macrophages play a key role in vocal fold fibrosis.

Introduction

Voice disorders worsen the quality of life by impairing communication and social functioning, which negatively affect mental health[1,2]. Vocal fold (VF) scarring, which occurs following inflammation, injury, and surgical resection, can cause irreversible voice impairment[3,4]. This results from excessive extracellular matrix (ECM) collagen deposition in the lamina propria, causing scarring and abnormal VF vibration[5,6]. Fibroblasts are the main producers of ECM[7], and previous studies targeting fibrosis prevention have primarily focused on them[8–11]. Treatments using growth factors and stem cells prevent fibrosis to some extent[10,12–14], however, they have not resulted in ideal tissue repair.

Fibrosis is an outcome of inflammatory and repair responses, and recent studies have demonstrated that macrophages are involved in both[15–17]. They change from pro- to anti-inflammatory phenotype during the wound healing process[18], contributing to the development of pathological fibrosis in various organs and injury models[16]. Therefore, we hypothesized that fibrosis could be regulated by controlling the macrophage phenotype, which functions as the key driver. Macrophages also interact with VF fibroblasts[19] and VF-derived mesenchymal stem cells[20,21] *in vitro*.

Peroxisome proliferator-activated receptor-γ (PPARγ) is a transcription factor that is prominently expressed by macrophages during early wound healing[22], regulating the phenotype. PPARγ activation suppresses the macrophage pro-inflammatory (M1-like)

phenotype under Th1 and Th17 polarizing conditions and promotes the anti-inflammatory/reparative (M2-like) phenotype under Th2[23].

Pioglitazone (PIO), a PPARγ agonist, is an antidiabetic drug in clinical use and has anti-inflammatory and anti-fibrotic effects in various disease models[24,25]. However, no studies have focused on the macrophage phenotype that prevents VF scar formation *in vivo*. Therefore, this study aimed to evaluate the effect of PIO, a macrophage phenotype regulator, on fibrosis in a rat model of VF injury.

Materials and Methods

Animals

Male Sprague-Dawley rats (350–450 g) were purchased from Shimizu Laboratory Supplies Co., Ltd. (Kyoto, Japan). The 13-week-old rats underwent surgical and injection procedures, while naïve (uninjured and untreated) ones were age-matched in each experiment. The rats were housed in a specific pathogen-free environment under controlled temperature, humidity, and light, and were given standard rodent food and water *ad libitum*. No rats died during the observation period. All the protocols and procedures were compliant with the Guidelines for the Proper Conduct of Animal Experiments of the Science Council of Japan. Ethical approval was obtained from the Animal Research Committee of Kyoto University (approval number: MedKyo20137).

Surgical procedure

The rat VF injury model is often used as a preclinical model for VF fibrosis[5,26]. Bilateral VF mucosal injuries were performed transorally, as previously described[26,27]. The rats were anesthetized with an intraperitoneal injection of 2.5 mg/kg butorphanol (Meiji Seika Pharma Co., Ltd., Tokyo, Japan), 2.0 mg/kg midazolam (Astellas Pharma Inc., Tokyo, Japan), and 0.15 mg/kg medetomidine (Nippon Zenyaku Kogyo Co., Ltd., Fukushima, Japan). They were then placed in a near-vertical position on a custom-made operating table. The larynx was observed with a 1.9 mm diameter, 30-degree rigid endoscope (Hopkins Telescope 1232BA, Karl Storz, Tuttlingen, Germany). The bilateral VFs were stripped with a custom-made 0.2 mm diameter tip needle[28] until the VF thyroarytenoid muscle was exposed.

Drug treatment

PIO (P1901, Tokyo Chemical Industry, Tokyo, Japan) and GW9662 (M6191; Sigma-Aldrich, St. Louis, MO, USA) were dissolved in saline containing 0.5% dimethyl sulfoxide. The rats were randomly assigned to treatment with 5 μM PIO, 50 μM PIO, 50 μM PIO with GW9662 or vehicle (0.5% dimethyl sulfoxide). Bilateral VF injections were administered on days 1, 3, 5, and 7 post-injury (Figure 1), using 10 μL microsyringes with a 33 G needle (Hamilton Company, Reno, NV). Animal positions and injection techniques were based on previous studies[29]. VFs were observed using a rigid endoscope under general anesthesia, as described above.

Histology and indirect immunofluorescence

Larynges were harvested at days 4 and 56 post-injury, corresponding to the inflammatory and scar maturation phases of wound healing in the rat model, respectively[26,27,30]. Rats were deeply anesthetized with pentobarbital and transcardially perfused with phosphate-buffered saline (PBS) followed by 4% paraformaldehyde. Larynges were dissected, placed in 4% paraformaldehyde overnight at 4 °C, and were then incubated in graded sucrose solutions overnight at 4 °C again. Tissues were snap-frozen in the optimum cutting temperature compound (Sakura Finetek, Torrance, CA). Serial 8 μm sections were cut in a cryostat and stored at -80 °C. Coronal sections containing laryngeal alar cartilage were used to assess the center of the injury, as previously described[27]. Five rats each were assigned to all the experimental groups, and one sample per rat was employed for each analysis. One sample each from the PIO 5 μM and PIO 50 μM groups at 56 days after injury was excluded from the analysis owing to insufficient dehydration and fixation before sectioning.

Routine hematoxylin and eosin (H&E), Masson's trichrome, and Alcian blue (pH 2.5, with and without hyaluronidase digestion) histological staining were performed to evaluate morphology, collagen abundance, and hyaluronic acid (HA), respectively.

For indirect immunofluorescence, the sections were boiled in citrate buffer (0.01 M, pH 6.0) for antigen retrieval, permeabilized, and blocked with 5% normal donkey serum (NDS), 1% bovine serum albumin (BSA), and 0.2% Triton X-100 in PBS for 1 hour at room

temperature. They were subsequently incubated with primary antibodies in PBS containing 2% NDS and 1% BSA overnight at 4 °C. Sections were washed three times, 5 minutes each, with PBS and incubated with secondary antibodies diluted in blocking buffer (2% NDS and 1% BSA) at 1:500 for 1 hour at room temperature. Nuclei were stained with 4',6-diamidino-2-phenylindole (DAPI). The slides were washed three times with PBS and mounted with Fluoromount-G (Thermo Fisher, Waltham, MA, USA).

Antibodies

Indirect immunofluorescence was performed using CD68 as a pan-macrophage marker, inducible nitric oxide synthase (iNOS) as pro-inflammatory (M1-like), and CD206 as anti-inflammatory (M2-like) macrophage markers, as previously described[31,32]. The three primary antibodies (CD68, iNOS, and CD206) were applied simultaneously.

The primary antibodies used were anti-rat CD68 (mouse, 1:1000, MCA341GA, Serotec, Oxford, UK), anti-iNOS (rabbit, 1:50, PA1-036, Invitrogen, Carlsbad, CA, USA), anti-mouse MMR/CD206 (goat, 1:250; AF2535, R&D Systems, Minneapolis, MN, USA), anti-collagen I (rabbit, 1:100, ab34710, Abcam, Cambridge, UK), and anti-fibronectin (mouse, 1:100, ab6328, Abcam). The secondary antibodies used were donkey anti-mouse Alexa 488, donkey anti-rabbit Alexa 488, donkey anti-rabbit Alexa 568, donkey anti-mouse Alexa 568, and donkey anti-goat Alexa 647 (Invitrogen).

Microscopy and image analysis

Images were obtained at × 40 magnification using a BZ-X710 all-in-one microscope (Keyence Co., Osaka, Japan). The investigators were blinded to the experimental group during image analysis. The lamina propria was defined as the area between the basement membrane and the thyroarytenoid muscle in the coronal section of the VFs. BZ-X analyzer software (Keyence) was used to count the number of stained cells and measure the area with the same threshold determined for each staining. The threshold value for a positive result was determined based on the background signal intensity and the negative control for each staining.

To evaluate the polarization of M1 and M2, we counted the number of cells with specific marker positivity. M1-like macrophages were defined as $iNOS^+$ $CD68^+$ cells, whereas M2-like ones were defined as $CD206^+$ $CD68^+$cells. The number of macrophages, including M1-like and M2-like ones, were manually counted. H&E staining was used to measure the area of VF lamina propria. The positive area ratio of Masson trichrome staining, Alcian blue staining, and immunostaining for collagen I and fibronectin were analyzed.

RNA isolation and quantitative real-time polymerase chain reaction (RT-PCR) (*in vivo*)

VF mucosa samples were collected as previously described[33]. Total RNA was isolated using the RNeasy Micro kit (Qiagen, Valencia, CA, USA) with on-column DNase I (Qiagen) digestion according to the manufacturer's instructions. RNA concentration and purity were determined using a spectrophotometer (ND-1000; NanoDrop, Wilmington, DE,

USA). cDNA was synthesized using a High-Capacity cDNA Reverse Transcription Kit (Applied Biosystems, Foster City, CA, USA) according to the manufacturer's instructions. Five rats each were assigned to all the experimental groups, and one sample per rat was used for each analysis. One sample each from the vehicle and PIO 50 μM + GW9662 groups was excluded from the analysis because of suspected contamination during RNA isolation. Quantitative RT-PCR was performed on a StepOnePlus RT-PCR system (Applied Biosystems) using THUNDERBIRD Probe qPCR Mix (Toyobo, Osaka, Japan) and TaqMan gene expression assay (Thermo Fisher), according to the manufacturer's instructions. Each assay was performed in duplicate or triplicate. The expression levels of each gene were normalized to the levels of *Sdha*[34] and analyzed using the ΔΔCt method[35]. The following probes were used: *Il1b* (R n00580432_m1), *Tnf* (Rn99999017_m1), *Arg1* (Rn00691090_m1), *Tgfb1* (Rn00572010_m1), *Cd68* (Rn01495634_g1), *Cd36* (Rn00580728_m1), *Ccl2* (Rn00580555_m1), *Col1a1* (Rn01463848_m1), *Fn1* (Rn00569575_m1), *Acta2* (Rn01759928_g1), *Il10* (Rn00563409_m1), *Has1* (Rn00597231_m1), *Has2* (Rn00565774_m1), and *Sdha* (Rn00590475_m1).

Cell culture

Human monocytic THP-1 (American Type Culture Collections, Rockville, MD, USA) cells were maintained in suspension culture in RPMI 1640 (30264-85, Nacalai Tesque, Kyoto, Japan) supplemented with 10% fetal bovine serum (CCP-FBS-BR-500, Cosmo Bio

Co., Tokyo, Japan), 100 U/ml penicillin and 100 μg/ml streptomycin solution (26253-84, Nacalai Tesque), and 0.05 mM 2-mercaptoethanol (21985-023, Thermo Fisher). THP-1 cells were differentiated into M0 macrophages by treatment with 100 ng/mL phorbol 12-myristate 13-acetate (PMA) (P1585; Sigma-Aldrich) for 96 h. These cells were divided into four groups: M0, M1, M1 + PIO, and M1 + PIO + GW9662. M0 macrophages were preincubated with GW9662 (10 μM; M6191; Sigma-Aldrich) or vehicle for 1 hour, then with PIO (10 μM; E6910; Sigma-Aldrich) or vehicle for another 2 hours. After 3 hours of preincubation, cells were co-stimulated with 1 μg/ml lipopolysaccharide (LPS) (E. coli O111: B4 L2630, Sigma-Aldrich) plus 20 ng/ml interferon (IFN)-γ (AF-300-02, PeproTech, Cranbury, NJ, USA) for 6 hours to generate inflammatory macrophages[36]. Cells were lysed with RNA lysis buffer to perform quantitative PCR analyses. All the experiments were performed as 5 independent experiments.

RNA isolation and quantitative PCR (*in vitro*)

Total RNA from the cells was isolated using the RNeasy mini kit (Qiagen) according to the manufacturer's instructions. The RNA concentration and purity were assessed by an ultraviolet spectrophotometer. Total RNA (1 μg) was reverse-transcribed using ReverTra Ace qPCR RT Master Mix with gDNA Remover (Toyobo). Quantitative PCR was performed on a QuantStudio 3 Real-Time PCR system (Applied Biosystems) using THUNDERBIRD Probe qPCR Mix (Toyobo) and TaqMan gene expression assay (Thermo Fisher), according to

the manufacturer's instructions. Each assay was performed in triplicate. The expression levels of each gene were normalized to the levels of *Gapdh* and analyzed using the ΔΔCt method. The following probes were used: *Il1b* (Hs01555410_m1), *Tnf* (Hs00174128_m1), *Ccl2* (Hs00234140_m1), and *Gapdh* (Hs99999905_m1).

Statistical Analysis

Statistical analyses and graphic representations were conducted using GraphPad Prism version 9.3.0 (GraphPad Software, San Diego, CA, USA). The mean values and standard error of the mean were calculated. Each data point derived from the quantitative PCR assays represents an average of 2 or 3 technical replicates, and data were averaged over independently replicated experiments (n = 4–5 independently collected samples) and analyzed by one-way analysis of variance followed by post-hoc Dunnett's test for comparison with the vehicle-treated control group. *P* values of $*P < 0.05$, $**P < 0.01$, $***P < 0.001$, were selected to indicate statistical significance.

Results

PIO reduces injury-induced macrophage accumulation

In the rat VF injury model, macrophages increased in the lamina propria on days 1 – 5 after injury[10]. The effects of PIO on macrophage infiltration were observed at day 4 after injury in the VF lamina propria. Indirect immunofluorescence revealed that PIO reduced the

injury-induced increase in density of CD68+ macrophages (Figure 2A, B). Quantitative RT-PCR demonstrated that PIO inhibited the injury-induced increase in *Cd68* and *Ccl2* gene expression. This effect of PIO was abolished by GW9662 (Figure 2C).

PIO inhibits injury-induced increase in M1-like macrophages

To assess the effects of PIO on macrophage phenotypes at day 4 after injury, pro-inflammatory M1-like and reparative M2-like macrophages were immunostained with iNOS and CD206, respectively (Figure 3A, D). PIO attenuated the injury-induced increase in density of $iNOS^+$ macrophages (Figure 3B). Moreover, 5 μM PIO, but not 50 μM PIO, suppressed the injury-induced increase in density of $CD206^+$ macrophages (Figure 3C). In the naïve VF, the majority of macrophages consisted of $iNOS^-$ $CD206^+$ macrophages (60%), and there were few $iNOS^+$ $CD206^-$ macrophages (4.1%). Following injury, the percentage of $iNOS^-$ $CD206^+$ macrophages markedly decreased (20.1%), and that of $iNOS^+$ $CD206^-$ macrophages (19.7%) and $iNOS^-$ $CD206^-$ macrophages (36.1%) increased. PIO treatment increased the percentage of $iNOS^-$ $CD206^+$ macrophages (PIO 50 μM, 33.7%) and decreased that of $iNOS^+$ $CD206^-$ macrophages (PIO 50 μM, 9.9%). $iNOS^+$ $CD206^+$ macrophages were present in all the experimental groups (Figure 3E).

Quantitative RT-PCR was performed to examine the expression of genes related to pro- and anti-inflammatory mediators. Gene expression of *Il1b*, *Tnf*, *Il10*, *Arg1*, and *Cd36* was not significantly different in the PIO (50 μM) and GW9662+PIO (50 μM) groups

compared to the vehicle group (Figure 4A).

PIO treatment attenuates fibrosis

To evaluate the anti-fibrotic effect of PIO, the expression of fibrosis-related factors and ECM components in the VF lamina propria was evaluated. Quantitative RT-PCR revealed that PIO inhibited the injury-induced increase in expression of *Tgfb1* and *Acta2* and the effect of PIO was inhibited by GW9662. PIO inhibited the injury-induced increase in *Fn1* expression, however, the effect of PIO was not abrogated by GW9662 (Figure 4B). The effect of PIO on *Col1a1* expression was not significant.

Indirect immunofluorescence indicated that PIO inhibited the injury-induced increase in the percentage of collagen type 1 (Figure 5A) and fibronectin (Figure 5B)-positive areas, and the effect of PIO was reversed by GW9662. Masson's trichrome staining revealed that PIO inhibited the injury-induced increase in the percentage of collagen deposition, and the effect of PIO was abrogated by GW9662 (Figure 5C).

PIO prevents contracture and hyaluronic acid level reduction in the VF lamina propria

The degree of atrophy in the VF lamina propria was assessed by the cross-sectional area on day 56 after injury. H&E staining revealed that PIO inhibited the injury-induced decrease in cross-sectional area, and GW9662 reversed the effect of PIO (Figure 5D). Alcian blue staining revealed that 50 μM PIO inhibited the injury-induced decrease in HA level, and the effect of PIO was reversed by GW9662 (Figure 5E). Moreover, 50 μM PIO inhibited the

injury-induced increase in Has1 expression, and GW9662 reversed the effect of PIO (Figure 4B).

PIO prevents LPS/IFN-γ-induced upregulation of *Ccl2* in THP-1-derived macrophages

To evaluate the effect of PIO on human macrophages, the expression of *Ccl2*, *Il1b*, and *Tnf* in THP-1-derived macrophages under LPS/IFNγ stimulation was examined by quantitative PCR. PIO inhibited the LPS/IFN-γ-induced increase in *Ccl2* expression in THP-1-derived macrophages, but the effect of PIO was not reversed by GW9662. PIO enhanced the LPS/IFN-γ-induced increase in *Il1b* expression in THP-1-derived macrophages, and GW9662 reversed the effect of PIO (Figure 6).

Discussion

This study evaluated the effects of PIO, a PPARγ agonist, on macrophage infiltration and phenotype, and tissue repair following VF injury. Results showed that PIO suppressed inflammatory macrophage accumulation and ECM-related gene expression in the acute phase. Furthermore, PIO inhibits fibrosis, contractures, and HA loss in the VF lamina propria during the scar maturation phase via PPARγ. These findings suggest that treatments targeting inflammatory macrophages or PPARγ activation in macrophages may prevent VF fibrosis.

Macrophages contribute to both inflammation and repair in the wound healing process. Depletion experiments in various organs have been performed using knockout mice

or liposomal clodronate, and revealed that macrophages are involved in fibrosis[37–39]. Although drug-induced fibrosis has been ameliorated by macrophage withdrawal during the fibrotic phase, injury-induced fibrosis, which has been tested primarily in the skin, has been reduced within 7 days during the acute phase[40,41]. Macrophage function in VFs has not been investigated in detail, however, a transient increase in iNOS-positive inflammatory macrophages has been reported from days 1 to 5 after injury[42]. Therefore, the therapeutic strategy in this study was focused on controlling inflammatory macrophages within 7 days of the acute phase. As expected, PIO treatment reduced the accumulation of macrophages, especially inflammatory macrophages, in the acute phase. However, unexpectedly, PIO treatment did not suppress the expression of *Il1b* and *Tnf*, which are upregulated in M1 macrophages[43].

PIO inhibited the injury-induced upregulation of *Ccl2* expression via PPARγ *in vivo* and LPS/IFNγ-induced upregulation of *Ccl2* expression in a PPARγ-independent manner *in vitro*. These results are consistent with previous findings that PIO reduces CCL2 production[44,45]. *Ccl2* is transcriptionally regulated by NFκB[46,47]. PPARγ ligands repress the transcriptional activity of NFκB and NFκB target genes in macrophages in a PPARγ-dependent[48,49] or PPARγ-independent manner[50,51], depending on their concentration and the stimulus applied to macrophages[52]. It is noteworthy that PIO repressed the expression of *Ccl2* in both *in vivo* experiments in rats and *in vitro* experiments in human macrophages, however,

noted that the signaling pathway of PIO could be different owing to the diverse conditions of the two experiments.

PIO inhibited the injury-induced upregulation of fibrosis-related genes and fibrosis, and *Ccl2* may be associated with this effect of PIO. *Ccl2* is reported to recruit and locally proliferate bone marrow-derived monocytes and macrophages via activation of C-C chemokine receptor type 2 (CCR2)[53,54]. iNOS$^+$ macrophages differentiate from bone marrow-derived monocytes in a CCR2-dependent manner[55]. These findings suggest that PIO reduces the accumulation of iNOS$^+$ macrophages by inhibiting *Ccl2* expression. Furthermore, studies using lung and heart injury models have revealed that bone marrow-derived macrophages lack repair capacity, whereas tissue-resident macrophages exhibit excellent repair capacity[56,57]. Based on these findings, PIO could exhibit improved repair capacity by preventing the accumulation of bone marrow-derived macrophages that lack repair capacity, resulting in reduced fibrosis and preserved HA. Further studies using genetic phylogenetic tracking techniques are needed. *Ccl2* has also been reported to amplify the expression of *Tgfb1* in human monocytes through autocrine and paracrine effects with TGF-β1[58]. In the VFs, TGF-β1 differentiates fibroblasts into myofibroblasts[59], induce a contractile phenotype[7], and upregulate the expression of *Fn1*, *Acta2*[60], and *Has1*[61]. Thus, suppression of *TGF-β1* expression via *Ccl2* by PIO may have inhibited the initiation of the fibrotic cascade, resulting in reduced tissue contraction. It is important to note that VF atrophy can cause dysphonia,

based on the size of the glottal gap during phonation[62].

This study had several limitations. PIO treatment may affect cells other than macrophages, as PPARγ agonists have been reported to act on adipocytes[63,64], fibroblasts[65,66], T cells[67], and vascular smooth muscle cells[68]. However, PPARγ is mainly expressed by macrophages during the inflammatory phase of wound healing[22]. Furthermore, studies using macrophage-specific PPARγ knockout mice have revealed that PIO treatment exerts its anti-inflammatory[69–71] and anti-fibrotic[71,72] effects by acting on PPARγ in macrophages. Therefore, the effect of PIO treatment in this study appears to be mainly due to its effects on the macrophages. Flow cytometry analysis of VF mucosal cells may be useful in assessing the changes in the functional phenotype of macrophages and other cell populations localized to the wound. Moreover, adoptive transfer of treated macrophages may be useful to evaluate the effects of PIO focusing only on macrophages.

In this study, sex differences were not examined. Previous studies have suggested that the pharmacokinetics of PIO may differ between males and females[73]. Furthermore, PPARγ expression is affected by sex hormones[74] and the sexual cycle[75]. Therefore, only male rats were used in this study to eliminate the effects of sex differences and sexual cycle. It remains unclear whether the effect of PIO on the macrophages differs between males and females. Hence, further research is warranted.

In summary, results of this study suggest that PIO inhibits the accumulation of

inflammatory macrophages in the early stage of wound healing and consequently prevents fibrosis during the scar maturation phase in a rat VF injury model. These effects may be due to the modulation of *Ccl2* expression in macrophages by PIO. Inflammatory macrophages and PPARγ activation may be potential targets for the treatment of VF fibrosis.

Acknowledgments

The authors thank the Center for Anatomical, Pathological, and Forensic Medical Research, Kyoto University Graduate School of Medicine, for preparing the microscope slides. Image analyses using a BZ-X710 all-in-one microscope were performed at the Medical Research Support Center, Graduate School of Medicine, Kyoto University, which was supported by the Platform for Drug Discovery, Informatics, and Structural Life Science from the Ministry of Education, Culture, Sports, Science and Technology, Japan.

References

1. Rosen CA, Lee AS, Osborne J, Zullo T, Murry T: Development and Validation of the Voice Handicap Index-10: The Laryngoscope 2004, 114:1549–1556.

2. Cohen SM, Dupont WD, Courey MS: Quality-of-Life Impact of Non-Neoplastic Voice Disorders: A Meta-Analysis. Ann Otol Rhinol Laryngol 2006, 115:128–134.

3. Woo P, Casper J, Colton R, Brewer D: Diagnosis and treatment of persistent dysphonia after laryngeal surgery: A retrospective analysis of 62 patients. The Laryngoscope 1994, 104:1084–1091.

4. Hirano S, Minamiguchi S, Yamashita M, Ohno T, Kanemaru S, Kitamura M: Histologic Characterization of Human Scarred Vocal Folds. J Voice 2009, 23:399–407.

5. Welham NV, Montequin DW, Tateya I, Tateya T, Choi SH, Bless DM: A Rat Excised Larynx Model of Vocal Fold Scar. J Speech Lang Hear Res 2009, 52:1008–1020.

6. Hansen JK, Thibeault SL: Current Understanding and Review of the Literature: Vocal Fold Scarring. J Voice 2006, 20:110–120.

7. Kishimoto Y, Kishimoto AO, Ye S, Kendziorski C, Welham NV: Modeling fibrosis using fibroblasts isolated from scarred rat vocal folds. Lab Invest 2016, 96:807–816.

8. Hirano S, Bless D, Heisey D, Ford C: Roles of hepatocyte growth factor and transforming growth factor beta1 in production of extracellular matrix by canine vocal fold fibroblasts. The Laryngoscope

2003, 113:144–148.

9. Suehiro A, Hirano S, Kishimoto Y, Tateya I, Rousseau B, Ito J: Effects of Basic Fibroblast Growth Factor on Rat Vocal Fold Fibroblasts. Ann Otol Rhinol Laryngol 2010, 119:690–696.

10. Chang Z, Kishimoto Y, Hasan A, Welham NV: TGF- 3 modulates the inflammatory environment and reduces scar formation following vocal fold mucosal injury in rats. Dis Model Mech 2014, 7:83–91.

11. Hiwatashi N, Bing R, Kraja I, Branski RC: Mesenchymal stem cells have antifibrotic effects on transforming growth factor-β1-stimulated vocal fold fibroblasts: MSCs Antifibrotic Effects on TGF-β1-Stimulated VFFs. The Laryngoscope 2017, 127:E35–E41.

12. Hirano S, Bless DM, Rousseau B, Welham N, Montequin D, Chan RW, Ford CN: Prevention of Vocal Fold Scarring by Topical Injection of Hepatocyte Growth Factor in a Rabbit Model: The Laryngoscope 2004, 114:548–556.

13. Suzuki R, Kawai Y, Tsuji T, Hiwatashi N, Kishimoto Y, Tateya I, Nakamura T, Hirano S: Prevention of vocal fold scarring by local application of basic fibroblast growth factor in a rat vocal fold injury model: Prevention of Vocal Fold Scarring by bFGF. The Laryngoscope 2017, 127:E67–E74.

14. Svensson B, Nagubothu RS, Cedervall J, Le Blanc K, Ährlund-Richter L, Tolf A, Hertegård S: Injection of human mesenchymal stem cells improves healing of scarred vocal folds: Analysis using a xenograft model. The Laryngoscope 2010, 120:1370–1375.

15. Henderson NC, Rieder F, Wynn TA: Fibrosis: from mechanisms to medicines. Nature 2020, 587:555–566.

16. Wynn TA, Vannella KM: Macrophages in Tissue Repair, Regeneration, and Fibrosis. Immunity 2016, 44:450–462.

17. Vannella KM, Wynn TA: Mechanisms of Organ Injury and Repair by Macrophages. In: Julius D, editor. Annu Rev Physiol Vol 79, Palo Alto, Annual Reviews, 2017, pp. 593–617.

18. Varga T, Mounier R, Horvath A, Cuvellier S, Dumont F, Poliska S, Ardjoune H, Juban G, Nagy L, Chazaud B: Highly Dynamic Transcriptional Signature of Distinct Macrophage Subsets during Sterile Inflammation, Resolution, and Tissue Repair. J Immunol 2016, 196:4771–4782.

19. King SN, Chen F, Jetté ME, Thibeault SL: Vocal fold fibroblasts immunoregulate activated macrophage phenotype. Cytokine 2013, 61:228–236.

20. King SN, Hanson SE, Chen X, Kim J, Hematti P, Thibeault SL: *In vitro* characterization of macrophage interaction with mesenchymal stromal cell-hyaluronan hydrogel constructs: Macrophage Interaction with MSC-Hydrogel Constructs. J Biomed Mater Res A 2014, 102:890–902.

21. Hanson SE, King SN, Kim J, Chen X, Thibeault SL, Hematti P: The Effect of Mesenchymal Stromal Cell–Hyaluronic Acid Hydrogel Constructs on Immunophenotype of Macrophages. Tissue Eng Part A 2011, 17:2463–2471.

22. Chen H, Shi R, Luo B, Yang X, Qiu L, Xiong J, Jiang M, Liu Y, Zhang Z, Wu Y: Macrophage peroxisome proliferator-activated receptor γ deficiency delays skin wound healing through impairing apoptotic cell clearance in mice. Cell Death Dis 2015, 6:e1597–e1597.

23. Lawrence T, Natoli G: Transcriptional regulation of macrophage polarization: enabling diversity with identity. Nat Rev Immunol 2011, 11:750–761.

24. Tokutome M, Matoba T, Nakano Y, Okahara A, Fujiwara M, Koga J-I, Nakano K, Tsutsui H, Egashira K: Peroxisome proliferator-activated receptor-gamma targeting nanomedicine promotes cardiac healing after acute myocardial infarction by skewing monocyte/macrophage polarization in preclinical animal models. Cardiovasc Res 2019, 115:419–431.

25. Lefere S, Puengel T, Hundertmark J, Penners C, Frank AK, Guillot A, de Muynck K, Heymann F, Adarbes V, Defrêne E, Estivalet C, Geerts A, Devisscher L, Wettstein G, Tacke F: Differential effects of selective- and pan-PPAR agonists on experimental steatohepatitis and hepatic macrophages. J Hepatol 2020, 73:757–770.

26. Tateya T, Sohn JH, Tateya I, Bless DM: Histologic Characterization of Rat Vocal Fold Scarring. Ann Otol Rhinol Laryngol 2005, 114:183–191.

27. Ling C, Yamashita M, Waselchuk EA, Raasch JL, Bless DM, Welham NV: Alteration in cellular morphology, density and distribution in rat vocal fold mucosa following injury. Wound Repair Regen 2010, 18:89–97.

28. Yamashita M, Bless DM, Welham NV: Surgical Method to Create Vocal Fold Injuries in Mice. Ann Otol Rhinol Laryngol 2009, 118:131–138.

29. Hiwatashi N, Hirano S, Mizuta M, Tateya I, Kanemaru S, Nakamura T, Ito J: Adipose-derived stem cells versus bone marrow-derived stem cells for vocal fold regeneration: Comparison of ASC and BMSC. The Laryngoscope 2014, 124:E461–E469.

30. Tateya I, Tateya T, Lim X, Sohn JH, Bless DM: Cell Production in Injured Vocal Folds: A Rat Study. Ann Otol Rhinol Laryngol 2006, 115:135–143.

31. Zhu M, Li W, Dong X, Yuan X, Midgley AC, Chang H, Wang Y, Wang H, Wang K, Ma PX, Wang H, Kong D: In vivo engineered extracellular matrix scaffolds with instructive niches for oriented tissue regeneration. Nat Commun 2019, 10:4620.

32. Venosa A, Malaviya R, Choi H, Gow AJ, Laskin JD, Laskin DL: Characterization of Distinct Macrophage Subpopulations during Nitrogen Mustard–Induced Lung Injury and Fibrosis. Am J Respir Cell Mol Biol 2016, 54:436–446.

33. Mizuta M, Hirano S, Hiwatashi N, Tateya I, Kanemaru S, Nakamura T, Ito J: Effect of astaxanthin on vocal fold wound healing. The Laryngoscope 2014, 124:E1–E7.

34. Chang Z, Ling C, Yamashita M, Welham NV: Microarray-driven validation of reference genes for quantitative real-time polymerase chain reaction in a rat vocal fold model of mucosal injury. Anal

Biochem 2010, 406:214–221.

35. Livak KJ, Schmittgen TD: Analysis of Relative Gene Expression Data Using Real-Time Quantitative PCR and the 2−ΔΔCT Method. Methods 2001, 25:402–408.

36. Chanput W, Mes JJ, Savelkoul HFJ, Wichers HJ: Characterization of polarized THP-1 macrophages and polarizing ability of LPS and food compounds. Food Funct 2013, 4:266–276.

37. Duffield JS, Forbes SJ, Constandinou CM, Clay S, Partolina M, Vuthoori S, Wu S, Lang R, Iredale JP: Selective depletion of macrophages reveals distinct, opposing roles during liver injury and repair. J Clin Invest 2005, 115:56–65.

38. Gibbons MA, MacKinnon AC, Ramachandran P, Dhaliwal K, Duffin R, Phythian-Adams AT, van Rooijen N, Haslett C, Howie SE, Simpson AJ, Hirani N, Gauldie J, Iredale JP, Sethi T, Forbes SJ: Ly6Chi monocytes direct alternatively activated profibrotic macrophage regulation of lung fibrosis. Am J Respir Crit Care Med 2011, 184:569–581.

39. Lin SL, Castaño AP, Nowlin BT, Lupher ML, Duffield JS: Bone marrow Ly6Chigh monocytes are selectively recruited to injured kidney and differentiate into functionally distinct populations. J Immunol 2009, 183:6733–6743.

40. Lucas T, Waisman A, Ranjan R, Roes J, Krieg T, Müller W, Roers A, Eming SA: Differential Roles of Macrophages in Diverse Phases of Skin Repair. J Immunol 2010, 184:3964–3977.

41. Mirza R, DiPietro LA, Koh TJ: Selective and specific macrophage ablation is detrimental to wound healing in mice. Am J Pathol 2009, 175:2454–2462.

42. Kaba S, Nakamura R, Yamashita M, Katsuno T, Suzuki R, Tateya I, Kishimoto Y, Omori K: Alterations in macrophage polarization in injured murine vocal folds. The Laryngoscope 2019, 129:E135–E142.

43. Mantovani A, Sica A, Sozzani S, Allavena P, Vecchi A, Locati M: The chemokine system in diverse forms of macrophage activation and polarization. Trends Immunol 2004, 25:677–686.

44. Kume O, Takahashi N, Wakisaka O, Nagano-Torigoe Y, Teshima Y, Nakagawa M, Yufu K, Hara M, Saikawa T, Yoshimatsu H: Pioglitazone attenuates inflammatory atrial fibrosis and vulnerability to atrial fibrillation induced by pressure overload in rats. Heart Rhythm 2011, 8:278–285.

45. Dasu MR, Park S, Devaraj S, Jialal I: Pioglitazone inhibits Toll-like receptor expression and activity in human monocytes and db/db mice. Endocrinology 2009, 150:3457–3464.

46. Ueda A, Ishigatsubo Y, Okubo T, Yoshimura T: Transcriptional regulation of the human monocyte chemoattractant protein-1 gene. Cooperation of two NF-kappaB sites and NF-kappaB/Rel subunit specificity. J Biol Chem 1997, 272:31092–31099.

47. Hildebrand DG, Alexander E, Hörber S, Lehle S, Obermayer K, Münck N-A, Rothfuss O, Frick J-S, Morimatsu M, Schmitz I, Roth J, Ehrchen JM, Essmann F, Schulze-Osthoff K: IκBζ Is a Transcriptional Key Regulator of CCL2/MCP-1. J Immunol 2013, 190:4812–4820.

48. Ricote M, Li AC, Willson TM, Kelly CJ, Glass CK: The peroxisome proliferator-activated receptor-gamma is a negative regulator of macrophage activation. Nature 1998, 391:79–82.

49. Pascual G, Fong AL, Ogawa S, Gamliel A, Li AC, Perissi V, Rose DW, Willson TM, Rosenfeld MG, Glass CK: A SUMOylation-dependent pathway mediates transrepression of inflammatory response genes by PPAR-gamma. Nature 2005, 437:759–763.

50. Chawla A, Barak Y, Nagy L, Liao D, Tontonoz P, Evans RM: PPAR-gamma dependent and independent effects on macrophage-gene expression in lipid metabolism and inflammation. Nat Med 2001, 7:48–52.

51. Straus DS, Pascual G, Li M, Welch JS, Ricote M, Hsiang CH, Sengchanthalangsy LL, Ghosh G, Glass CK: 15-deoxy-delta 12,14-prostaglandin J2 inhibits multiple steps in the NF-kappa B signaling pathway. Proc Natl Acad Sci U S A 2000, 97:4844–4849.

52. Welch JS, Ricote M, Akiyama TE, Gonzalez FJ, Glass CK: PPARgamma and PPARdelta negatively regulate specific subsets of lipopolysaccharide and IFN-gamma target genes in macrophages. Proc Natl Acad Sci U S A 2003, 100:6712–6717.

53. Tsou C-L, Peters W, Si Y, Slaymaker S, Aslanian AM, Weisberg SP, Mack M, Charo IF: Critical roles for CCR2 and MCP-3 in monocyte mobilization from bone marrow and recruitment to inflammatory sites. J Clin Invest 2007, 117:902–909.

54. Pang J, Maienschein-Cline M, Koh TJ: Enhanced Proliferation of Ly6C+ Monocytes/Macrophages Contributes to Chronic Inflammation in Skin Wounds of Diabetic Mice. J Immunol 2021, 206:621–630.

55. Menezes S, Melandri D, Anselmi G, Perchet T, Loschko J, Dubrot J, Patel R, Gautier EL, Hugues S, Longhi MP, Henry JY, Quezada SA, Lauvau G, Lennon-Duménil A-M, Gutiérrez-Martínez E, Bessis A, Gomez-Perdiguero E, Jacome-Galarza CE, Garner H, Geissmann F, Golub R, Nussenzweig MC, Guermonprez P: The Heterogeneity of Ly6Chi Monocytes Controls Their Differentiation into iNOS+ Macrophages or Monocyte-Derived Dendritic Cells. Immunity 2016, 45:1205–1218.

56. Lavine KJ, Epelman S, Uchida K, Weber KJ, Nichols CG, Schilling JD, Ornitz DM, Randolph GJ, Mann DL: Distinct macrophage lineages contribute to disparate patterns of cardiac recovery and remodeling in the neonatal and adult heart. Proc Natl Acad Sci U S A 2014, 111:16029–16034.

57. Misharin AV, Morales-Nebreda L, Reyfman PA, Cuda CM, Walter JM, McQuattie-Pimentel AC, Chen C-I, Anekalla KR, Joshi N, Williams KJN, Abdala-Valencia H, Yacoub TJ, Chi M, Chiu S, Gonzalez-Gonzalez FJ, Gates K, Lam AP, Nicholson TT, Homan PJ, Soberanes S, Dominguez S, Morgan VK, Saber R, Shaffer A, Hinchcliff M, Marshall SA, Bharat A, Berdnikovs S, Bhorade SM, Bartom ET, Morimoto RI, Balch WE, Sznajder JI, Chandel NS, Mutlu GM, Jain M, Gottardi CJ, Singer BD, Ridge KM, Bagheri N, Shilatifard A, Budinger GRS, Perlman H: Monocyte-derived alveolar macrophages drive lung fibrosis and persist in the lung over the life span. J Exp Med 2017, 214:2387–2404.

58. Sakai N, Wada T, Furuichi K, Shimizu K, Kokubo S, Hara A, Yamahana J, Okumura T, Matsushima K, Yokoyama H, Kaneko S: MCP-1/CCR2-dependent loop for fibrogenesis in human peripheral CD14-positive monocytes. J Leukoc Biol 2006, 79:555–563.

59. Vyas B, Ishikawa K, Duflo S, Chen X, Thibeault SL: Inhibitory effects of hepatocyte growth factor and interleukin-6 on transforming growth factor-beta1 mediated vocal fold fibroblast-myofibroblast differentiation. Ann Otol Rhinol Laryngol 2010, 119:350–357.

60. Nakamura R, Mukudai S, Bing R, Garabedian MJ, Branski RC: Complex fibroblast response to glucocorticoids may underlie variability of clinical efficacy in the vocal folds. Sci Rep 2020, 10:20458.

61. Lim X, Bless DM, Muñoz-Del-Río A, Welham NV: Changes in cytokine signaling and extracellular matrix production induced by inflammatory factors in cultured vocal fold fibroblasts. Ann Otol Rhinol Laryngol 2008, 117:227–238.

62. Omori K, Slavit DH, Matos C, Kojima H, Kacker A, Blaugrund SM: Vocal fold atrophy: quantitative glottic measurement and vocal function. Ann Otol Rhinol Laryngol 1997, 106:544–551.

63. Tontonoz P, Hu E, Graves RA, Budavari AI, Spiegelman BM: mPPAR gamma 2: tissue-specific regulator of an adipocyte enhancer. Genes Dev 1994, 8:1224–1234.

64. Sandouk T, Reda D, Hofmann C: Antidiabetic agent pioglitazone enhances adipocyte differentiation of 3T3-F442A cells. Am J Physiol 1993, 264:C1600-1608.

65. Milam JE, Keshamouni VG, Phan SH, Hu B, Gangireddy SR, Hogaboam CM, Standiford TJ, Thannickal VJ, Reddy RC: PPAR-gamma agonists inhibit profibrotic phenotypes in human lung fibroblasts and bleomycin-induced pulmonary fibrosis. Am J Physiol Lung Cell Mol Physiol 2008, 294:L891-901.

66. Ghosh AK, Bhattacharyya S, Lakos G, Chen S-J, Mori Y, Varga J: Disruption of transforming growth factor beta signaling and profibrotic responses in normal skin fibroblasts by peroxisome proliferator-activated receptor gamma. Arthritis Rheum 2004, 50:1305–1318.

67. Klotz L, Burgdorf S, Dani I, Saijo K, Flossdorf J, Hucke S, Alferink J, Nowak N, Novak N, Beyer M, Mayer G, Langhans B, Klockgether T, Waisman A, Eberl G, Schultze J, Famulok M, Kolanus W, Glass C, Kurts C, Knolle PA: The nuclear receptor PPAR gamma selectively inhibits Th17 differentiation in a T cell-intrinsic fashion and suppresses CNS autoimmunity. J Exp Med 2009, 206:2079–2089.

68. Law RE, Goetze S, Xi XP, Jackson S, Kawano Y, Demer L, Fishbein MC, Meehan WP, Hsueh WA: Expression and function of PPARgamma in rat and human vascular smooth muscle cells. Circulation 2000, 101:1311–1318.

69. Hucke S, Floßdorf J, Grützke B, Dunay IR, Frenzel K, Jungverdorben J, Linnartz B, Mack M, Peitz M, Brüstle O, Kurts C, Klockgether T, Neumann H, Prinz M, Wiendl H, Knolle P, Klotz L: Licensing of myeloid cells promotes central nervous system autoimmunity and is controlled by peroxisome proliferator-activated receptor γ. Brain J Neurol 2012, 135:1586–1605.

70. Abdullah Z, Geiger S, Nino-Castro A, Böttcher JP, Muraliv E, Gaidt M, Schildberg FA, Riethausen K, Flossdorf J, Krebs W, Chakraborty T, Kurts C, Schultze JL, Knolle PA, Klotz L: Lack of PPARγ in myeloid cells confers resistance to Listeria monocytogenes infection. PloS One 2012, 7:e37349.

71. Morán-Salvador E, Titos E, Rius B, González-Périz A, García-Alonso V, López-Vicario C, Miquel R, Barak Y, Arroyo V, Clària J: Cell-specific PPARγ deficiency establishes anti-inflammatory and anti-fibrogenic properties for this nuclear receptor in non-parenchymal liver cells. J Hepatol 2013, 59:1045–1053.

72. Caglayan E, Stauber B, Collins AR, Lyon CJ, Yin F, Liu J, Rosenkranz S, Erdmann E, Peterson LE, Ross RS, Tangirala RK, Hsueh WA: Differential roles of cardiomyocyte and macrophage peroxisome proliferator-activated receptor gamma in cardiac fibrosis. Diabetes 2008, 57:2470–2479.

73. Fujita Y, Yamada Y, Kusama M, Yamauchi T, Kamon J, Kadowaki T, Iga T: Sex differences in the pharmacokinetics of pioglitazone in rats. Comp Biochem Physiol Toxicol Pharmacol CBP 2003, 136:85–94.

74. Sato H, Sugai H, Kurosaki H, Ishikawa M, Funaki A, Kimura Y, Ueno K: The effect of sex hormones on peroxisome proliferator-activated receptor gamma expression and activity in mature adipocytes. Biol Pharm Bull 2013, 36:564–573.

75. Kadowaki K, Fukino K, Negishi E, Ueno K: Sex differences in PPARgamma expressions in rat adipose tissues. Biol Pharm Bull 2007, 30:818–820.

Figure legends

Figure 1. Experimental timeline

Schematic illustration of the injury, drug injection, and tissue collection schedule. Vehicle, pioglitazone 5 μM, pioglitazone 50 μM, or pioglitazone 50 μM with GW9662 were injected into the rat vocal folds (VFs) on days 1, 3, 5, and 7 after injury. VFs were harvested on days 4 and 56 after injury for indirect immunofluorescence, histology, and quantitative real-time polymerase chain reaction. Uninjured and untreated VFs were used as naïve controls.

Figure 2. Pioglitazone decreases macrophage accumulation in the vocal fold (VF) lamina propria on day 4 after injury. (A) Coronal sections of VF lamina propria on day 4 after injury were stained for CD68 (green) by indirect immunofluorescence. Nuclei were counterstained with 4',6-diamidino-2-phenylindole (blue). Representative images of $CD68^+$ macrophages are shown. The bottom panels show magnified images of the regions indicated by dashed boxes in the middle panels. **(B)** Quantification of the $CD68^+$ cells. **(C)** Quantitative real-time polymerase chain reaction analysis of mRNA levels of *Cd68* and *Ccl2* on day 4 after injury. Scale bars: 100 μm (**A, top and middle panels**); 50 μm (**A, bottom panels**). All data are presented as means ± standard error of the mean. n = 4–5 rats per group. $*P < 0.05$, $**P < 0.01$, $***P < 0.001$ compared with the vehicle-treated group.

Figure 3. Pioglitazone reduces the percentage of M1-like macrophages in the vocal fold (VF) lamina propria on day 4 after injury. Indirect immunofluorescence analysis of macrophage phenotypes in the coronal sections of the VF lamina propria on day 4 after injury. **(A)** Representative images of $CD68^+$ inducible nitric oxide synthase $(iNOS)^+$ (M1-like) macrophages. iNOS (red), CD68 (green), and 4',6-diamidino-2-phenylindole (DAPI) (blue). The bottom panels show magnified images of the regions indicated by the dashed boxes in the middle panels. **(B)** Quantitative analysis of the density of $CD68^+$ $iNOS^+$ (M1-like) macrophages. **(D)** Representative images of $CD68^+$ $CD206^+$ (M2-like) macrophages. CD206 (red), CD68 (green), and DAPI (blue). The bottom panels show magnified images of the regions indicated by the dashed boxes in the middle panels. **(C)** Quantitative analysis of the density of $CD68^+$ $CD206^+$ (M2-like) macrophages. **(E)** Stacked bar graphs show the proportions of $iNOS^-$ $CD206^-$, $iNOS^-$ $CD206^+$, $iNOS^+$ $CD206^+$, and $iNOS^+$ $CD206^-$ macrophages. Scale bars: 100 μm (**A and D, top and middle panels**); 20 μm (**A and D, bottom panels**). All the data are presented as means ± standard error of the mean. n = 5 rats per group. $*P < 0.05$, $***P < 0.001$ compared with the vehicle-treated group.

Figure 4. Effect of pioglitazone on the expression of genes related to inflammation and wound healing on day 4 after injury. (A) Quantitative real-time polymerase chain reaction (RT-PCR) analysis of gene expression related to M1/M2 polarization. mRNA expression

levels of IL-1β, TNF, Arg1, IL-10, and CD36 were measured. (B) Quantitative RT-PCR analysis of gene expression related to wound healing. mRNA expression levels of TGF-β1, Fn1, Acta2, Col-1a1, Has1, and Has2 were determined. All the data are presented as means ± standard error of the mean. n = 4–5 rats per group. **P* < 0.05, ***P* < 0.01, ****P* < 0.001 compared with the vehicle-treated group.

Figure 5. Pioglitazone inhibits fibrosis, tissue contracture, and hyaluronic acid loss in vocal fold (VF) lamina propria on day 56 after injury. Coronal sections of the VF lamina propria on day 56 after injury were analyzed. **(A)** Indirect immunofluorescence of type I collagen (red). **(B)** Indirect immunofluorescence of fibronectin (red). **(C)** Masson's trichrome staining for collagen (blue). **(D)** Hematoxylin and eosin staining. **(E)** Alcian blue staining of hyaluronic acid (light blue). Representative images (**left four panels**) and quantification of the percentage of the positive area (**right panel**) are shown. Scale bars: 200 μm. All the data are presented as means ± standard error of the mean. n = 4–5 rats per group. **P* < 0.05, ***P* < 0.01, ****P* < 0.001 compared with the vehicle-treated group.

Figure 6. Effects of pioglitazone on lipopolysaccharide (LPS) + interferon (IFN)-γ induced expression of *Ccl2*, *Il1b*, and *Tnf* in THP-1-derived macrophages

THP-1-derived macrophages (M0) were pretreated with or without GW9662 (10 μM) for 1

hour and then treated with pioglitazone (10 μM) for another 2 hours, followed by LPS + IFN-γ treatment for 6 hours. Expression of Ccl2, Il1b, and Tnf was assessed by quantitative polymerase chain reaction. All data are presented as means ± standard error of the mean. n = 5 per group. *P < 0.05, ***P < 0.001 compared with the vehicle-treated M1 macrophage group.

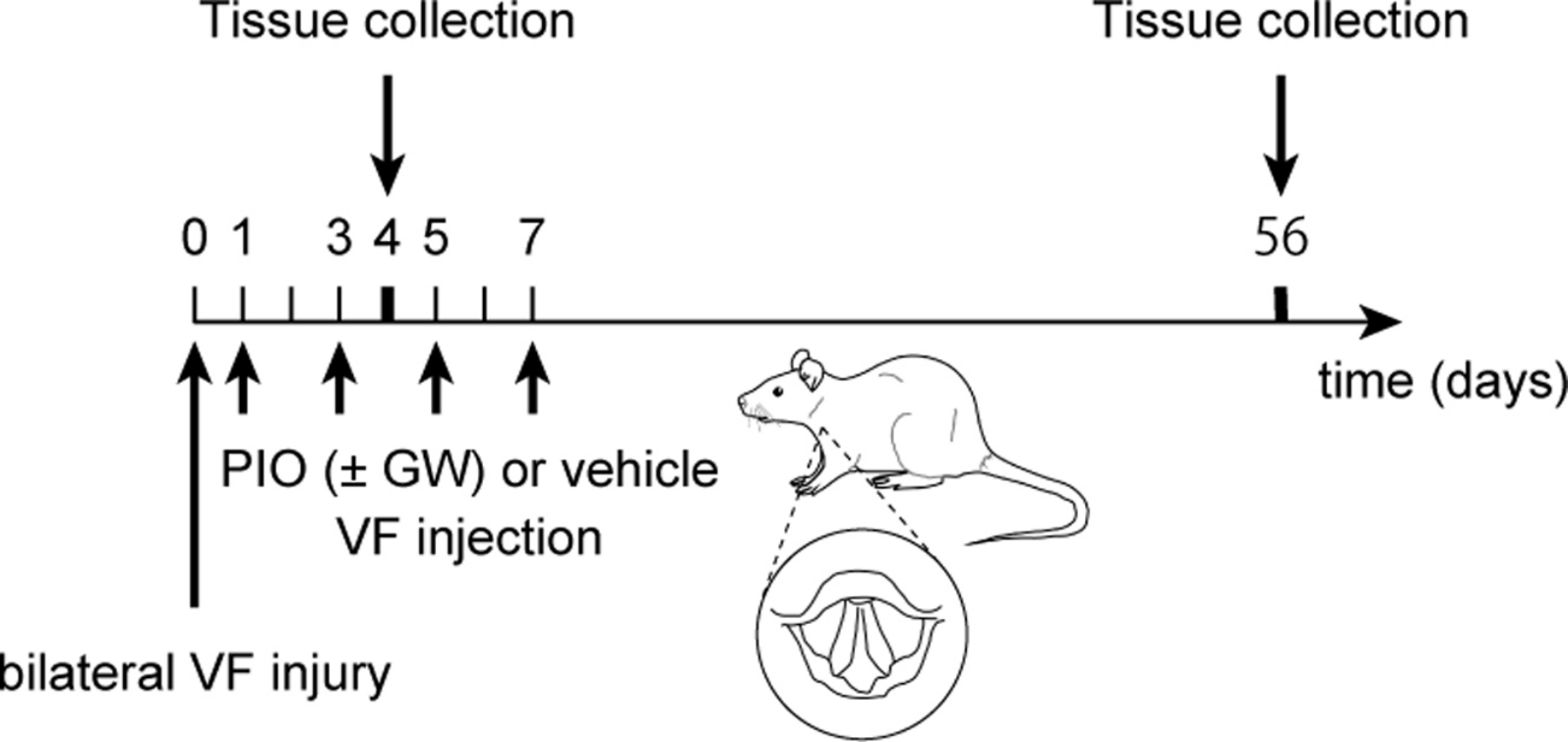
Tissue collection
Tissue collection
0 1 3 4 5 7
56
time (days)
PIO (± GW) or vehicle
VF injection
bilateral VF injury

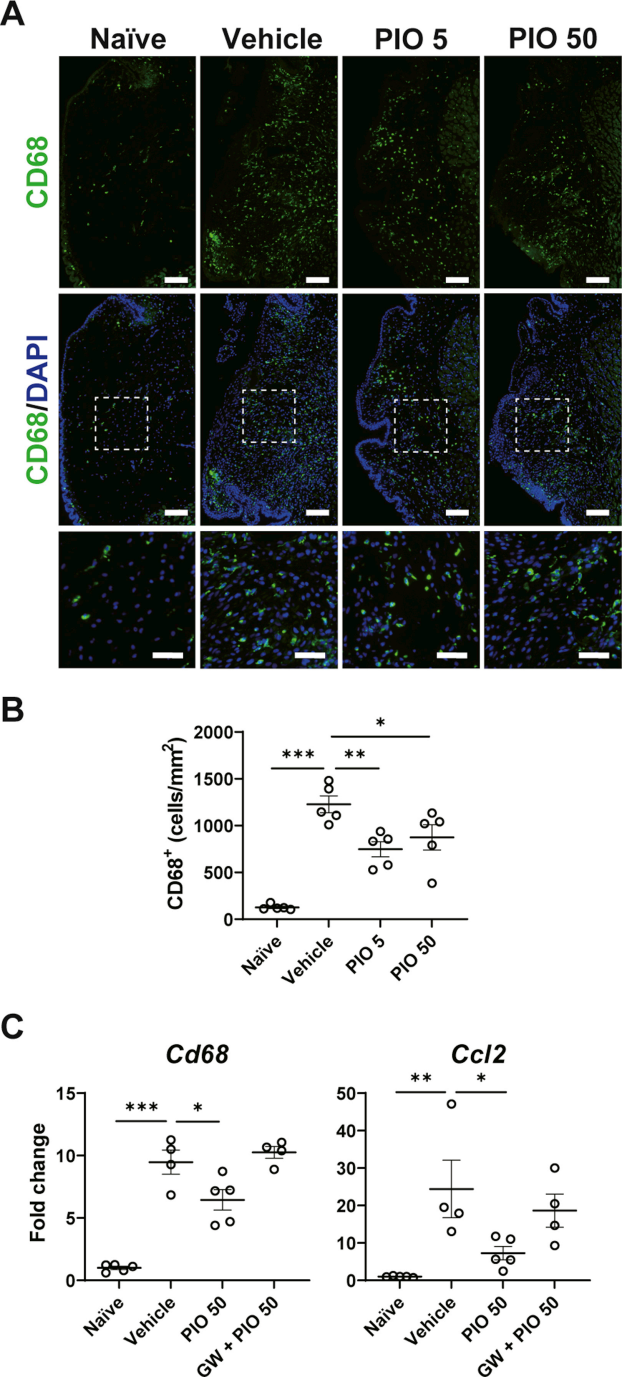
A
Naïve
Vehicle
PIO 5
PIO 50
CD68
CD68/DAPI
B
CD68+ (cells/mm2)
2000
1500
1000
500
0
***
**
*
Naïve
Vehicle
PIO 5
PIO 50
C
Cd68
Ccl2
Fold change
15
10
5
0
50
40
30
20
10
0
***
*
**
*
Naïve
Vehicle
PIO 50
GW + PIO 50

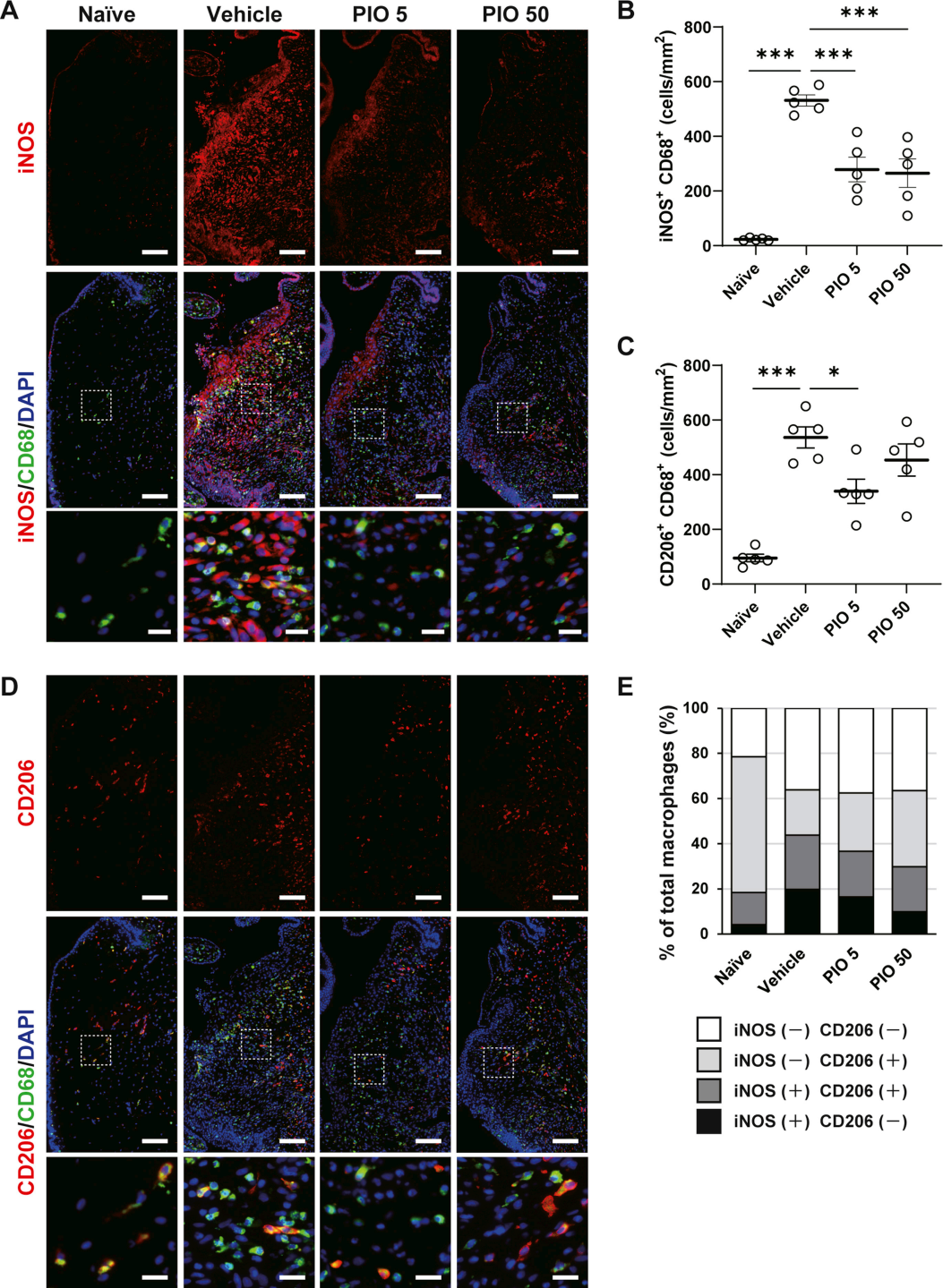
A
Naïve
Vehicle
PIO 5
PIO 50
iNOS
iNOS/CD68/DAPI
B
iNOS+ CD68+ (cells/mm2)
800
600
400
200
0
***
***
***
Naïve
Vehicle
PIO 5
PIO 50
C
CD206+ CD68+ (cells/mm2)
800
600
400
200
0
***
*
Naïve
Vehicle
PIO 5
PIO 50
D
CD206
CD206/CD68/DAPI
E
% of total macrophages (%)
100
80
60
40
20
0
Naïve
Vehicle
PIO 5
PIO 50
iNOS (−) CD206 (−)
iNOS (−) CD206 (+)
iNOS (+) CD206 (+)
iNOS (+) CD206 (−)

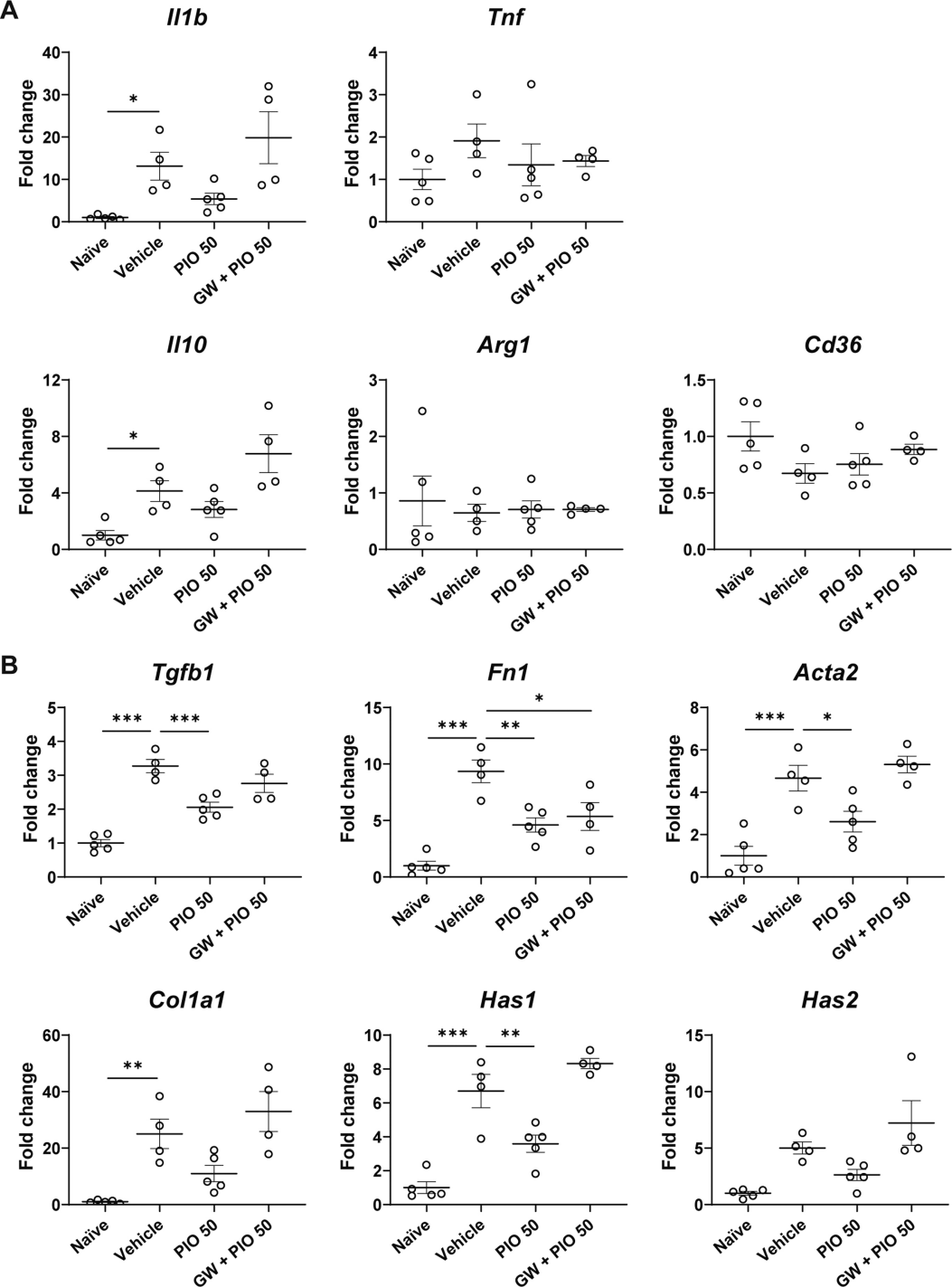
A
Il1b
Tnf
Il10
Arg1
Cd36
Fold change
Naïve
Vehicle
PIO 50
GW + PIO 50
B
Tgfb1
Fn1
Acta2
Col1a1
Has1
Has2

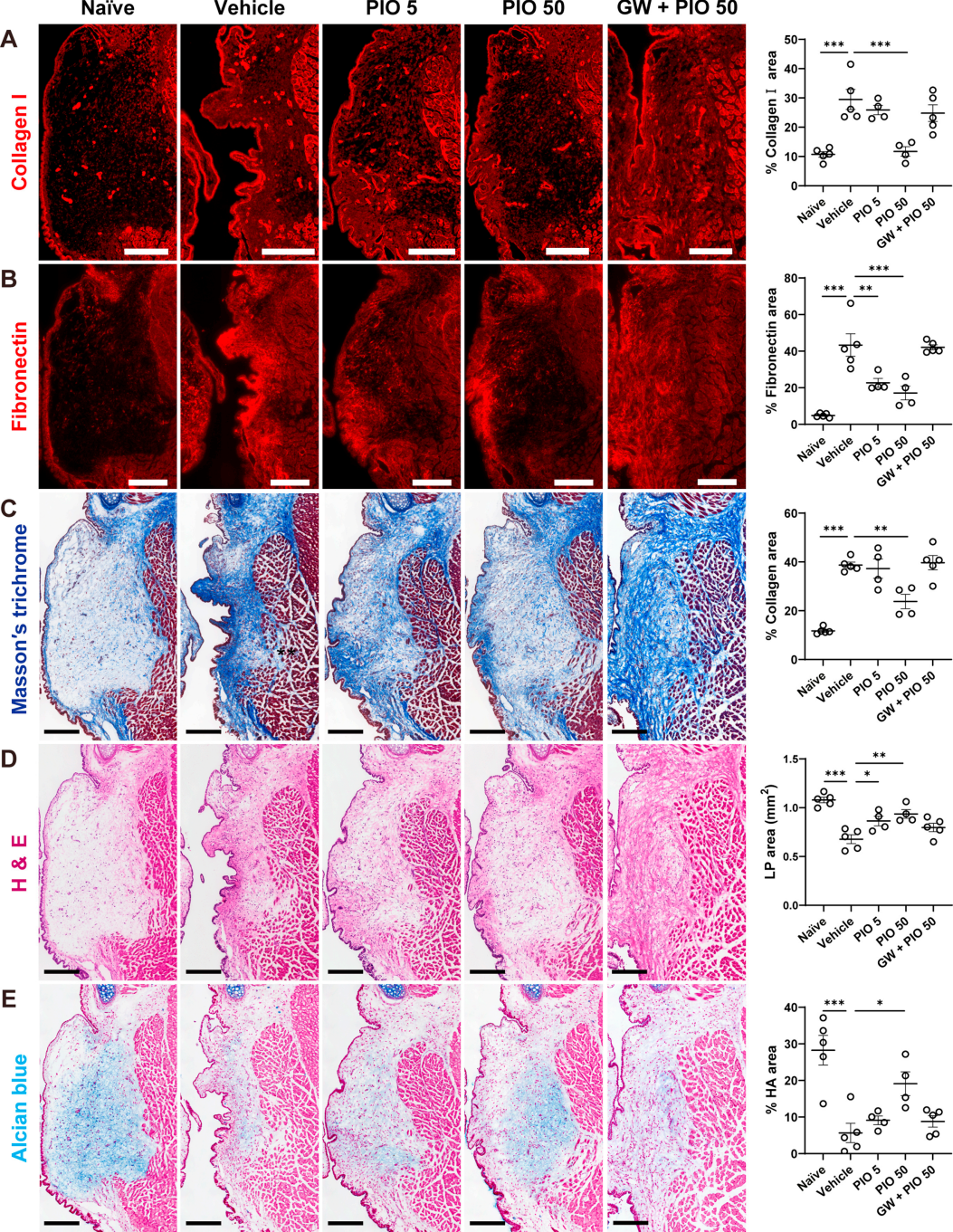
Naïve
Vehicle
PIO 5
PIO 50
GW + PIO 50
A
Collagen I
% Collagen I area
B
Fibronectin
% Fibronectin area
C
Masson's trichrome
% Collagen area
D
H & E
LP area (mm2)
E
Alcian blue
% HA area

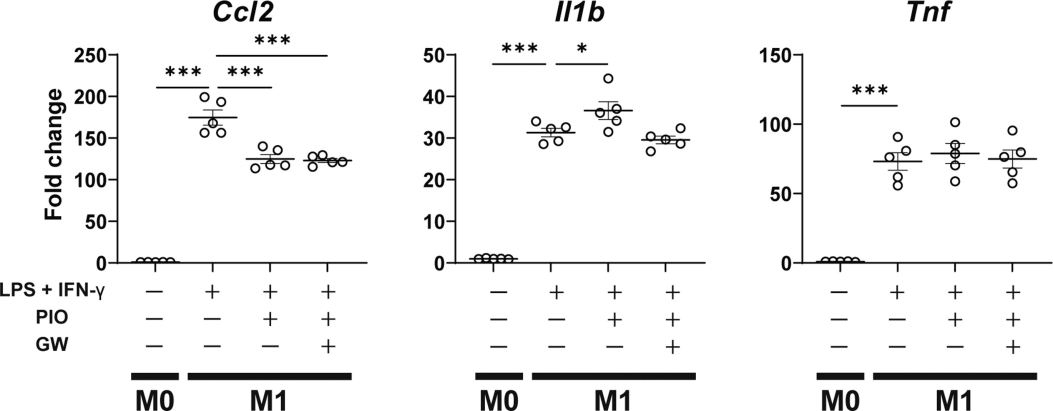
Ccl2
Il1b
Tnf
Fold change
250
200
150
100
50
0
50
40
30
20
10
0
150
100
50
0
***
***
***
***
*
***
LPS + IFN-γ
PIO
GW
M0
M1
M0
M1
M0
M1